# Adaptive Roll Autopilot Design for Interceptor Missile

Shivendra N. Tiwari
*Dept. of Electrical Eng.*
*Indian Institute of Technology*
Hyderabad, INDIA.
shivnath.tiwari@gmail.com

Ketan P. Detroja
*Dept. of Electrical Eng.*
*Indian Institute of Technology*
Hyderabad, INDIA.
ketan@ee.iith.ac.in

***Abstract*—Tactical missiles are designed to target a variety of aerial and ground objects, which can be stationary or moving. To effectively intercept these targets with minimal miss-distance, tactical missiles require a highly efficient control system. Obtaining a high level of accuracy in the aerodynamic characterization of the missile is notably challenging. In addition, the difficulty in modeling external disturbances complicates the autopilot design. As a result, there is a significant need for a robust control system that can handle parametric uncertainties and unmodeled external disturbances. This paper presents a robust roll autopilot based on the $\mathcal{L}_1$ adaptive technique. The proposed roll autopilot is designed to handle uncertainties, external disturbances, and unmodeled sensor delays. This approach treats both external disturbances and parametric uncertainties within the roll loop as composite disturbances. A state observer is used to estimate the composite disturbance, and the system states in a unified manner. The estimates obtained from the inner loop uncertainties are used to calculate the adaptive roll control input, which enhances the baseline control input designed for nominal operating conditions. Simulation results are provided to demonstrate the effectiveness of the adaptive roll autopilot in achieving the specified design objectives.**

*Keywords*: roll autopilot, $\mathcal{L}_1$ adaptive technique, non-linear six-degree-of-freedom interceptor model.

## I. Introduction

Tactical missiles are used against different types of targets, which range from stationary to highly maneuverable. The autopilot design should be highly efficient in hitting the target with an acceptable miss-distance. It is known that high-accuracy aerodynamic characterization of the missile is complicated. However, an accurate aerodynamic model of disturbance terms such as side force moment along pitch and yaw and induced rolling moment along the roll channel is challenging to establish aerodynamically, especially at different roll orientations and high angles of attack. In addition to that, tactical missiles tend to roll due to various undesirable rolling moments, such as those arising from airframe misalignment, asymmetric loading of the lifting and control surfaces, fin biases, and atmospheric disturbances. Incorporating a resolver onboard is essential for command-guided missiles due to their motion characteristics. However, this adds weight and complexity to the system. In contrast, homing missiles must maintain their roll angle within specific limits because of the asymmetrical look angle freedom of the seeker and the resulting image rotation relative to the pixel address.

In addition to stabilizing the roll position, limiting the roll rate in practical scenarios is crucial. Due to induced yaw rates, high roll rates can lead to difficulties with frame-to-frame correlation, de-centering errors, and gimbal angle saturation. Moreover, excessive roll rates can cause sensor saturation, potentially resulting in incorrect control inputs if the saturation persists for an extended period.

The designs based on classical approaches are presented in [1]. In [2], a nonlinear control law is proposed to stabilize the rolling motion while considering control cross-coupling. Additional examples include designs based on adaptive control [3], [4], the $H_\infty$ approach [5], $\mu$-synthesis [6], nonlinear dynamic inversion [7], [8], and nonlinear dynamic inversion combined with neural networks [9].

Recently, a robust roll autopilot design has been proposed using a disturbance estimation and rejection approach based on the extended-state-observer (ESO) technique, as discussed in [10], [11]. This approach treats the impact of external disturbances and parametric uncertainties in the roll loop as a composite or total disturbance. The ESO estimates both the disturbance and the system states, which are then utilized to enhance the robustness of a Linear Quadratic Regulator (LQR) controller designed for a nominal system.

In addition, variable structure control with sliding mode techniques has been employed to create robust roll control systems for tactical missiles. However, first-order sliding mode control often leads to a chattering phenomenon that adversely affects the actuator lifespan. To address this issue, higher-order sliding mode control has shown promise in mitigating chattering in various practical applications. For example, the super-twisting algorithm is applied to implement second-order sliding mode control [12]. This algorithm can function not only as a controller but also as an observer and a differentiator. Furthermore, the twisting algorithm, another second-order sliding mode method, has been used to enhance the roll control of missiles [13], accounting for dynamics associated with actuators and sensors.

In [14], a robust roll autopilot has been designed to reduce the couplings of a tactical missile. This paper applied the classic pole placement method to control the system, which was

linearized by feedback linearization. Furthermore, the aerodynamic couplings were compensated using nonlinear induced roll moment, and a model was introduced to control cross-coupling roll moment. Additionally, using the uncertainty and disturbance estimation technique, the controller will be robust against modeling errors, un-modeled dynamics, uncertainties in the aerodynamic coefficients, and external disturbances. In the research paper by [15], a nonlinear state feedback roll controller is designed using sum-of-squares optimization. The roll controller is designed based on a stability criterion, which can be viewed as a dual to Lyapunov's second theorem. This criterion has a convexity property, which is used for controller design with convex optimization.

This paper investigates realistic roll dynamics that include roll plant instability, primarily at high angles of attack. The design is validated in a high-fidelity six-degree-of-freedom environment, where various practical effects are considered, such as system nonlinearities, cross-coupling effects, control surface deflections, and rate limits and delays introduced by sampling and computation. This paper is organized as follows: Section II introduces the problem at hand, starting with formulating the interceptor roll channel. Section III presents the proposed designs for adaptive roll autopilots. In Section IV, we provide numerical simulation results and conduct robustness studies to assess parameter inaccuracy and unmodeled dynamics. These results demonstrate the effectiveness of the proposed autopilot designs. Finally, Section V concludes the paper.

## II. Problem Formulation

### A. Modeling of the Interceptor roll channel

The roll channel dynamic equation for high-angle-of-attack interceptor missiles can be expressed as a second-order differential equation. Usually, roll autopilots are designed by concentrating on rigid body dynamics while maintaining sufficient stability margins to account for the impact of unmodeled dynamics. The general aerodynamic model for roll dynamics can be formulated as follows

$$\begin{aligned} \dot{p} &= \frac{QSd}{I_{xx}}\left(-C_{rm} - \frac{C_{l_p}d}{2V_m}p - C_{l_\zeta}\delta_p\right) \\ &+ \frac{(I_{yy} - I_{zz})\,qr}{I_{xx}} \end{aligned} \tag{1}$$

It is evident from Fig. 1 that the aerodynamic roll angle ($\phi$) changes either due to the rotation of the body or the rotation of the velocity vector's projection. Assuming that the missile's total velocity ($V_T$) and total angle of attack ($\alpha$) remain constant, the projection of the missile's velocity vector remains fixed in an inertial frame. As a result, the following relationship will hold

$$\dot{\phi} = -p \tag{2}$$

Roll rate is considered positive if the rotation is anticlockwise about the body X-axis ($X_B$) and negative vice-versa. A new

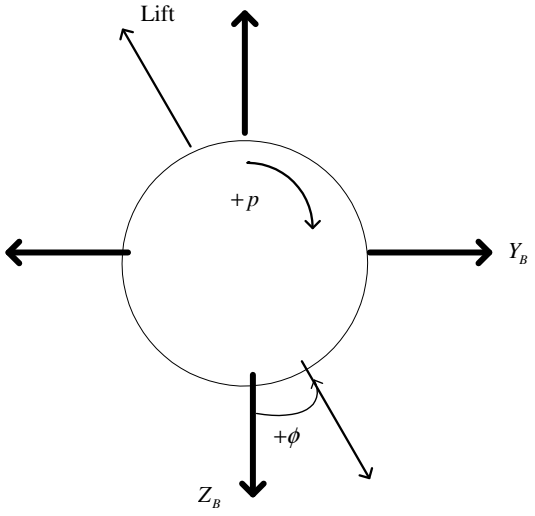


Fig. 1. Missile rear view: Roll Rate and $\phi$

variable $C_{r\phi}$ is introduced which is the partial derivative of $C_{rm}$ w.r.t. $\phi$ as

$$\begin{aligned} dC_{rm} &= \frac{\partial C_{rm}(M,\alpha,\phi)}{\partial \phi}d\phi \\ C_{rm} &= C_{r\phi}\phi \end{aligned} \tag{3}$$

Using the $C_{rm}$ data, slope is computed with respect to aerophi ($C_{r\phi}$).

$$C_{r\phi_i} = \frac{C_{rmi+1} - C_{rmi}}{\phi_{i+1} - \phi_i} \tag{4}$$

The dynamic derivative term in (1) provides the damping in roll channel. (1) can be rewritten by neglecting cross-coupling term as

$$-\ddot{\phi} = \frac{QSd}{I_{xx}}(-C_{r\phi}\phi + \frac{C_{l_p}d}{2V_m}\dot{\phi} - C_{l_\zeta}\delta_p) \tag{5}$$

$$I_{xx}\ddot{\phi} + QSd\frac{C_{l_p}d}{2V_m}\dot{\phi} - QSdC_{r\phi}\phi = QSdC_{l_\zeta}\delta_p \tag{6}$$

The dynamics of the roll channel can be represented as a transfer function by taking the Laplace transform on either side of the above equation

$$\frac{\phi(s)}{\delta_p(s)} = \frac{QSdC_{l_\zeta}}{I_{xx}s^2 + QSd\frac{C_{l_p}d}{2V_m}s - QSdC_{r\phi}} \tag{7}$$

Here, the actuator has been modeled as a second order system having transfer function as

$$\frac{\delta_p(s)}{\delta_{pc}(s)} = \frac{\omega_a^2}{s^2 + 2\varsigma_a\omega_a s + \omega_a^2} \tag{8}$$

where $\delta_{pc}$ is the commanded roll deflection, $\omega_a$ and $\varsigma_a$ are the natural frequency and damping ratio respectively of the actuator.

### B. Plant Instability

By neglecting the damping term $(C_{l_p})$ (very small value), the poles of the system can be found by equating $I_{xx}s^2 - QSdC_{r\phi} = 0$

$$s = \pm\sqrt{\frac{QSdC_{r\phi}}{I_{xx}}} \tag{9}$$

The placement of unstable poles on the pole-zero diagram is a significant concern in autopilot design. This necessitates the development of a roll autopilot with excellent disturbance rejection characteristics capable of limiting the peak roll rate within operational limits. When the slope of the roll disturbance moment coefficient $C_{rm}$ with respect to the aerodynamic roll angle $(\phi)$ is positive, it can create a positive feedback loop, leading to unstable roll dynamics. Unstable poles are calculated for various Mach numbers, angles of attack, and aerodynamic angles. An estimate of the maximum unstable pole is illustrated in Fig. 2. It is important to note that this figure does not display stable pole locations, which occur when $C_{r\phi}$ is negative. Consequently, including $C_{r\phi}$ can make the system highly unstable under certain operating conditions. Therefore, the objective in designing a roll autopilot is not to create a controller for an unstable plant but rather for a plant that transitions from stable to unstable dynamics as the aerodynamic roll angle changes.

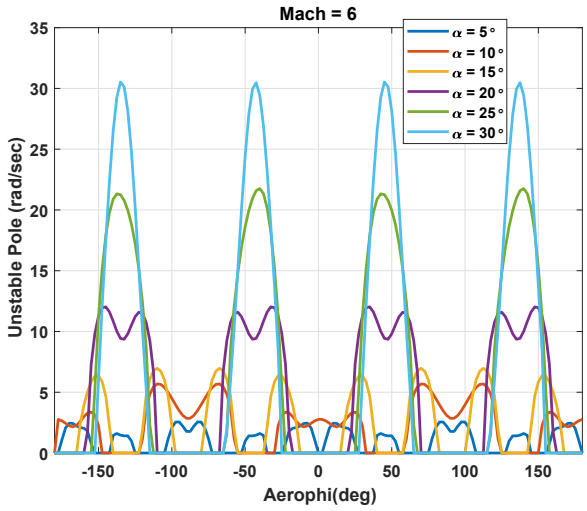


Fig. 2. Unstable Pole at Mach 6

## III. Roll Autopilot Designs

A roll autopilot design based on a rate gyro and employing a two-loop system has been considered, as illustrated in Fig. 3. In this design, the integrated roll rate (roll angle) serves as feedback in the outer loop, while the roll rate is used as feedback in the inner loop. The gains $K_{op}$ and $K_{ip}$ are applied in the outer and inner loops, respectively. A low-frequency lag-lead compensator must be designed to ensure the roll autopilot is insensitive to disturbances—the lag compensator aids in keeping the roll angle close to zero. The gains are iterated within a defined range, along with the plant pole in the right half of the s-plane (indicating an unstable pole). Stability margins are computed considering all plant perturbations for various levels of the unstable pole and the iterated control parameters. A control term is added to the baseline roll autopilot to estimate and compensate for roll disturbance moments. The outer loop roll autopilot equation is defined as follows.

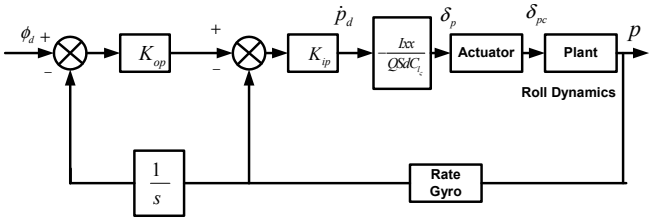


Fig. 3. Block Diagram of Baseline Roll Autopilot

$$p_d = K_{op}\left(\varphi_d - \int pdt\right) \tag{10}$$

$$\dot{p} = \dot{p}_d - K_{ip}\left(p - p_d\right) \tag{11}$$

The baseline roll control deflection command is defined as

$$\delta_{p_{bl}} = -\frac{Ixx}{QSdC_{l_\zeta}}\dot{p}_d \tag{12}$$

The baseline control law is augmented with an adaptive element $\delta_{p_{ad}}$. Adaptive augmentation used to augment baseline control is designed in the inner loop. A schematic of adaptive roll autopilot is shown in Fig. 4.

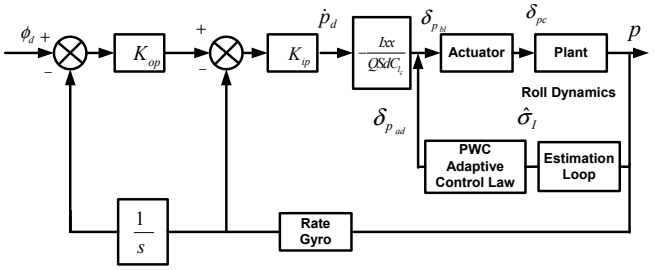


Fig. 4. A Schematic of Roll Autopilot with adaptive augmentation

*1) Mathematical Model for control design:* To simplify the algebra (1) of roll dynamics can be written in a simpler form as

$$\begin{aligned}\dot{p} &= \hat{A}_I(\wedge_I \delta_p + f_I) + \hat{B}_I \\ &= \hat{A}_I\left((\wedge_I - 1)\,\delta_p + f_I\right) + \hat{A}_I\delta_p + \hat{B}_I \\ &= \hat{A}_I\delta_p + \hat{B}_I + \sigma_I\end{aligned} \tag{13}$$

Where,

$$\hat{A}_I = \frac{QSd}{I_{xx}}$$
$$\wedge_I = -C_{l_\zeta}$$
$$\text{f\_I} = -C_{rm} - \frac{C_{l_p} d}{2V_m} p$$
$$\hat{B}_I = \frac{(I_{yy} - I_{zz})\, qr}{I_{xx}}$$

*2) Estimator for the Inner Loop:* The inner loop uncertainty $\sigma_I$ is estimated here. The state predictor for the inner loop can be given by,

$$\dot{\hat{p}} = \hat{A}_I \delta_p + \hat{B}_I + \hat{\sigma}_I - K_{e_p} \tilde{e}_p \quad (14)$$
$$\tilde{e}_p = \hat{p} - p \quad (15)$$

Where $\delta_p$ is the actual (achieved/sensed) roll control deflection $\hat{p}$ is the predictor roll rate and $\tilde{e}_p$ is the prediction roll rate error. $K_{e_p}$ is the gain for proportional state predictor respectively. $\hat{\sigma}_I$ are the uncertainty estimates.

$$\dot{\tilde{e}_p} = -K_{e_p} \tilde{e}_p + \hat{\sigma}_I - \sigma_I \quad (16)$$

Thus, as the estimator error tracks the actual error, predictor output tracks the actual output. Here, $K_{e_p}$ is the gain parameter which is used to design this tracking characteristics. Following procedures similar to [16], the derivation of uncertainty estimator is obtained. At any given time instant $iT_s$, the prediction error ($\tilde{e}_p$) can be calculated by comparing the current predicted output with the actual output. This error diminishes until the next update according to the dynamics of the prediction error described by equation (16). Consequently, the contribution of this error at the next update time $(i+1)T_s$ can be anticipated. In the Piecewise Constant (PWC) adaptation scheme, it is not feasible to precisely estimate the exact error $\tilde{e}_p((i+1)T_s)$ during the subsequent update. As a result, complete cancellation of the error is not achievable. However, the remaining error can be arbitrarily small by reducing the sample time $T_s$ since the unknown error occurs only between two updates. To address this known error, the following strategy has been formulated.

Solution of (16) in the continuous time domain can be written as,

$$\tilde{e}_p(t) = e^{-K_{e_p}(t-t_0)} \tilde{e}_p(t_0) + \int_{t_0}^{t} e^{-K_{e_p}(t-\tau)} (\hat{\sigma}_I - \sigma_I) d\tau \quad (17)$$

For the PWC adaptation law,

$$\tilde{e}_p(iT_s + \Delta t) = e^{-K_{e_p}\Delta t} \tilde{e}_p(iT_s) + \int_{iT_s}^{iT_s+\Delta t} e^{-K_{e_p}(iT_s+\Delta t-\xi)} (\hat{\sigma}_I - \sigma_I) d\xi \quad (18)$$

At the instant of next update,

$$\begin{aligned}\tilde{e}_p((i+1)T_s) &= e^{-K_{e_p}T_s} \tilde{e}_p(iT_s) + \int_{iT_s}^{(i+1)T_s} e^{-K_{e_p}((i+1)T_s-\xi)} (\hat{\sigma}_I - \sigma_I) d\xi \\ &= e^{-K_{e_p}T_s} \tilde{e}_p(iT_s) + \int_0^{T_s} e^{-K_{e_p}(T_s-\tau)} (\hat{\sigma}_I - \sigma_I) d\tau \\ &= e^{-K_{e_p}T_s} \tilde{e}_p(iT_s) + \int_0^{T_s} e^{-K_{e_p}(T_s-\tau)} \hat{\sigma}_I d\tau - \int_0^{T_s} e^{-K_{e_p}(T_s-\tau)} \sigma_I d\tau \end{aligned} \quad (19)$$

Because $\hat{\sigma}_I$ is constant over each sampling time, it can be taken out of the integration, to yield

$$\begin{aligned}\tilde{e}_p((i+1)T_s) &= e^{-K_{e_p}T_s} \tilde{e}_p(iT_s) + \left[\int_0^{T_s} e^{-K_{e_p}(T_s-\tau)} d\tau\right] \hat{\sigma}_I - \int_0^{T_s} e^{-K_{e_p}(T_s-\tau)} \sigma_I d\tau \\ &= e^{-K_{e_p}T_s} \tilde{e}_p(iT_s) - (-K_{e_p})^{-1} \left[1 - e^{-K_{e_p}T_s}\right] \hat{\sigma}_I - \int_0^{T_s} e^{-K_{e_p}(T_s-\tau)} \sigma_I d\tau \end{aligned} \quad (20)$$

To cancel the decaying prediction error at the next update,

$$e^{-\boldsymbol{K}_{e_p}T_s} \tilde{\boldsymbol{e}}_p(iT_s) - (-\boldsymbol{K}_{e_p})^{-1} \left[1 - e^{-\boldsymbol{K}_{e_p}T_s}\right] \hat{\boldsymbol{\sigma}}_{\boldsymbol{I}} = 0$$

By rearranging the terms $\hat{\sigma}_I$ can be obtained as

$$\hat{\sigma}_I = \left[(-K_{e_p})^{-1} \left(1 - e^{-K_{e_p}T_s}\right)\right]^{-1} e^{-K_{e_p}T_s} \tilde{e}_p(iT_s)$$

It can be written as

$$\begin{aligned}\hat{\sigma}_I(t) &= -\phi_I^{-1} \mu_I(iT_s), \quad t \in [iT_s, (i+1)T_s) \\ \phi_I &= (-K_{e_p})^{-1}(e^{-K_{e_p}T_s} - 1) \\ \boldsymbol{\mu}_I(iT_s) &= e^{-K_{e_p}T_s} \tilde{e}_p(iT_s) \end{aligned} \quad (21)$$

*3) Control Law Augmentation:* The inner loop uncertainty estimates are used to compute the adaptive roll control input, which is used to augment the baseline control input. To obtain the adaptive control input $\delta_{p_{AD}}$, (13) can be formulated as

$$\begin{aligned}\dot{p} &= \hat{A}_I \delta_p + \hat{B}_I + \sigma_I \\ &= \hat{B}_I + \hat{A}_I(\delta_{p_{bl}} + \delta_{p_{ad}}) + \sigma_I \\ &= \hat{B}_I + \hat{A}_I \delta_{p_{bl}} + \hat{A}_I \delta_{p_{ad}} + \sigma_I \end{aligned} \quad (22)$$

As $p_d \equiv p_{bl}$ and

$$\hat{B}_I + \hat{A}_I \delta_{p_{bl}} = \dot{p}_{bl} - K_{ip}(p - p_{bl}) \quad (23)$$

Apply this to (22) leads to,

$$\dot{p} \quad = \quad \dot{p}_{bl} - K_{ip}\left(p - p_{bl}\right) + \hat{A}_I \delta_{p_{ad}} + \sigma_I \tag{24}$$

For $p$ to track $p_{bl}$,

$$\dot{p} \quad = \quad \dot{p}_{bl} - K_{ip}\left(p - p_{bl}\right) \tag{25}$$

Hence,

$$\hat{A}_I \delta_{p_{ad}} + \sigma_I \quad = \quad 0$$

Thus, the adaptive roll control input can be obtained as

$$\delta_{p_{ad}} = \left(\hat{A}_I\right)^{-1} \hat{\sigma}_I \tag{26}$$

Adding the bandwidth limiting filter over the estimated inner loop uncertainty,

$$\delta_{p_{ad}} = C_I(s) \left(\hat{A}_I\right)^{-1} \hat{\sigma}_I \tag{27}$$

## IV. Simulation Results and Discussions

Simulations has been done for different initial conditions and angles of attack for proposed adaptive roll autopilot. Parametric uncertainties have been taken to be $\pm 20\%$ in all the cases.

### A. Case 1

In this case simulations has been done for varying angle of attack and fixed initial condition for proposed adaptive roll autopilot. Results for $\alpha = 15,\ 20,\ 25,\ 30deg$ and $\phi_0 = 10deg$ and $\dot{\phi}_0 = 0deg/s$ are shown in Fig. 5 and Fig. 6. The proposed adaptive roll autopilot is able to suppress roll rate independently of $\alpha$. The control trajectories and control efforts are shown in Fig. 7 for varying angle of attack.

### B. Case 2

In this case simulations has been done for constant angle of attack and varying initial conditions for proposed adaptive roll autopilot. The reference angle of attack is maintained at $\alpha = 30.0deg$ while the initial roll angle changes between $\phi_0 = 50deg$ and $\phi_0 = -40deg/s$. Initial roll rate is maintained at $\phi_0 = \dot{0}deg/s$. State trajectories are shown in Fig. 8 and Fig. 9 . The proposed adaptive roll autopilot is able to suppress roll rate independently of $\phi_0$. The control trajectories are shown in Fig. 10 for varying initial roll angle. As $|\phi_0|$ increases proposed adaptive roll autopilot controller apply more and more control input to drive the state to origin which is visible from the Fig. 10.

## V. Conclusion

Tactical missiles are designed to target both aerial and ground objects, necessitating precise control to minimize miss-distance. The complex aerodynamic characteristics and unmodeled external disturbances complicate roll autopilot design, highlighting the need for robust control. This paper presents a robust roll autopilot utilizing the $\mathcal{L}_1$ adaptive technique, designed to handle uncertainties, disturbances, and

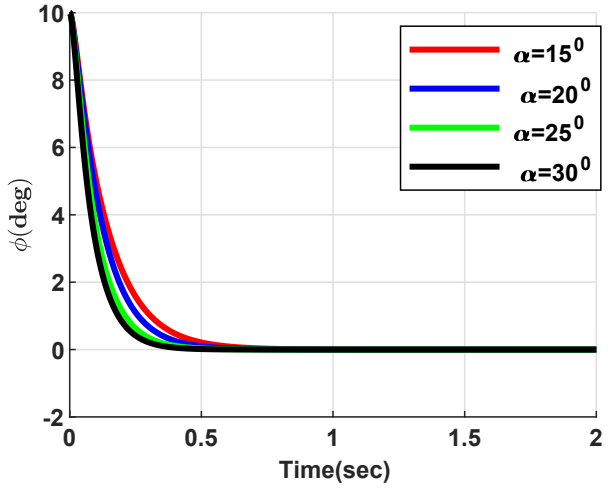


Fig. 5. Roll angle time history for $\alpha = 15°,\ 20°,\ 25°,\ 30°$

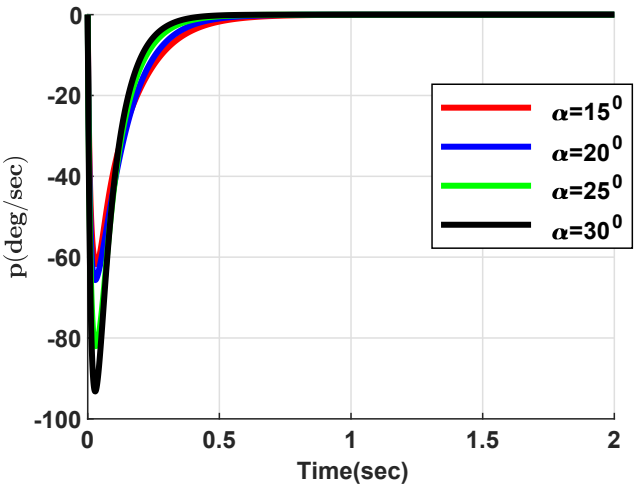


Fig. 6. Roll rate time history for $\alpha = 15°,\ 20°,\ 25°,\ 30°$

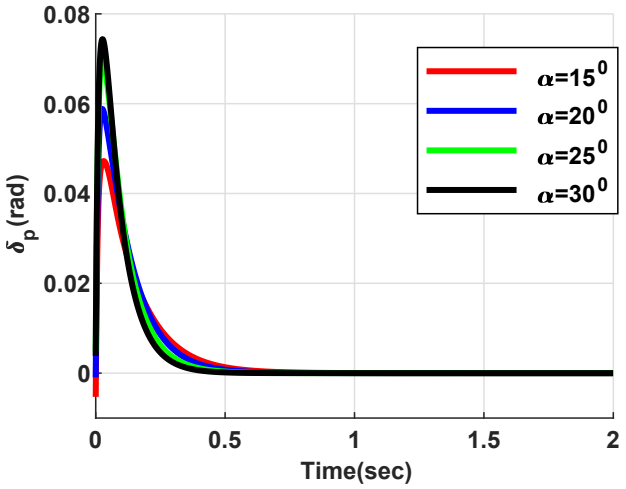


Fig. 7. A roll deflection time history for $\alpha = 15°,\ 20°,\ 25°,\ 30°$

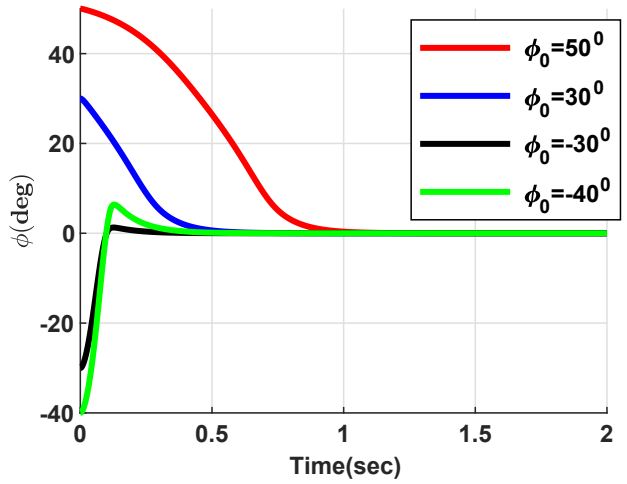


Fig. 8. Roll angle time history for $\phi_0 = 50°,\ 30°,\ -30°,\ -40°$

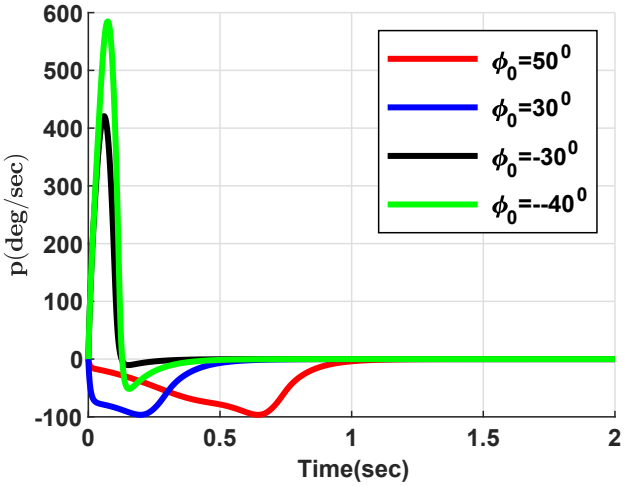


Fig. 9. Roll rate time history for $\phi_0 = 50°,\ 30°,\ -30°,\ -40°$

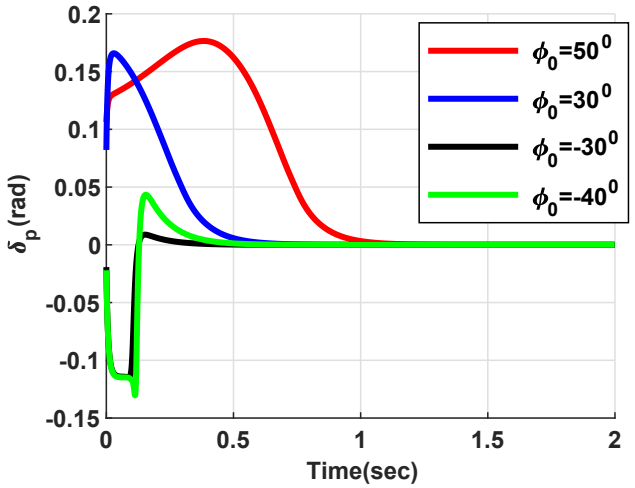


Fig. 10. A roll deflection time history for $\phi_0 = 50°,\ 30°,\ -30°,\ -40°$

sensor lags. The system employs a state observer to estimate composite disturbances and states, using inner-loop uncertainty estimates to enhance the baseline control input. Simulation results demonstrate the effectiveness of the adaptive roll autopilot in achieving design objectives.

## ACKNOWLEDGMENTS

The authors would like to sincerely thank Dr. Abhijit. Bhattacharya, Senior Scientist (DRDL, DRDO, India) for his support and encouragement for this research.

## REFERENCES

[1] P. Christopher, "Roll-attitude control of a missile having a strong aerodynamic non-linearity," *International Journal of Control*, vol. 31, no. 2, pp. 209–218, 1980.

[2] B.-E. Jun and C. Song, "A nonlinear roll autopilot based on 5-dof models of missiles," *IFAC Proceedings Volumes*, vol. 41, no. 2, pp. 14 029–14 035, 2008.

[3] D. Stallard, "A missile adaptive roll autopilot with a new dither principle," *IEEE Transaction of Automatic Control*, vol. 11, no. 3, pp. 368–378, 1966.

[4] P. Bendotti and M. M. Saad, "Multivariable adaptive control for the design of stt missile autopilots," *Control Engineering Practice*, vol. 1, no. 2, pp. 365–374, 1993.

[5] R. Colgren, "Nonlinear $h_\infty$ control of a missile's roll axis," in *American Control Conference*, Baltimore, MD, USA, June 1994, pp. 2109–2113.

[6] H. Buschek, "Full envelope missile autopilot design using gain scheduled robust control," *AIAA Joumal of Guidance, Control, and Dynamics*, vol. 22, pp. 115–122, 1999.

[7] P. K. Menon, M. E. Badget, R. A. Walker, and E. L. Duke, "Nonlinear flight test trajectory controllers for aircraft," *Joumal of Guidance, Control, and Dynamics*, vol. 10, no. 1, pp. 67–72, 1987.

[8] S. N. Tiwari, P. N. Dwivedi, and A. Bhattacharyya, "Robust scheduling of nonlinear time-scale separated autopilot using online static margin estimation," *IFAC-PapersOnLine*, vol. 51, no. 1, pp. 621–626, 2018.

[9] M. B. McFarland and A. J. Calise, "Adaptive nonlinear control of agile antiair missile using neural networks," *IEEE Transactions on Control System Technology*, vol. 8, no. 5, pp. 749–756, 2000.

[10] S. E. Talole, A. A. Godbole, J. P. Kolhe, and S. B. Phadke, "Robust roll autopilot design for tactical missiles," *Journal of guidance, control, and dynamics*, vol. 34, no. 1, pp. 107–117, 2011.

[11] C. V. Sirisha, R. Das, and S. E. Talole, "Performance investigation of extended-state-observer-based roll autopilot design," *Proceedings of the Institution of Mechanical Engineers, Part G: Journal of Aerospace Engineering*, vol. 229, no. 12, pp. 2205–2220, 2015.

[12] P. P. Parkhi, B. Bandyopadhyay, and M. Jha, "Roll autopilot design using second order sliding mode," *International Journal of Automation and Control*, vol. 7, no. 3, pp. 202–221, 2013.

[13] P. K. Trivedi, B. Bandyopadhyay, S. Mahata, and S. Chaudhuri, "Roll stabilization: a higher-order sliding-mode approach," *IEEE Transactions on Aerospace and Electronic Systems*, vol. 51, no. 3, pp. 2489–2496, 2015.

[14] M. R. Mohammadi, M. F. Jegarkandi, and A. Moarrefianpour, "Robust roll autopilot design to reduce couplings of a tactical missile," *Aerospace Science and Technology*, vol. 51, pp. 142–150, 2016.

[15] S. P. Khesal and I. Mohammadzaman, "Nonlinear robust roll autopilot design using sum-of-squares optimization," *Journal of Dynamic Systems, Measurement, and Control*, vol. 140, no. 11, p. 111005, 2018.

[16] M. Geiser, E. Xargay, N. Hovakimyan, T. Bierling, and F. Holzapfel, "L1 adaptive augmented dynamic inversion controller for a high agility uav," in *AIAA guidance, navigation, and control conference*, Portland, Oregon, USA, 2011, p. 6457.